

Adaptive Multirobot Formation Planning to Enclose and Track a Target with Motion and Visibility Constraints

Gonzalo López-Nicolás, Miguel Aranda and Youcef Mezouar

Abstract—Addressing the problem of enclosing and tracking a target requires multiple agents with adequate motion strategies. We consider a team of unicycle robots with a standard camera on board. The robots must maintain the desired enclosing formation while dealing with their nonholonomic motion constraints. The reference formation trajectories must also guarantee permanent visibility of the target by overcoming the limited field of view of the cameras. We present a novel approach to characterize the conditions on the robots’ trajectories taking into account the motion and visual constraints. We also propose online and offline motion planning strategies to address the constraints involved in the task of enclosing and tracking the target. These strategies are based on maintaining the formation shape with variable size or, alternatively, on maintaining the size of the formation with flexible shape.

I. INTRODUCTION

Many aspects and issues are involved in the topic of multi-robot systems. These systems bring the ability to collectively carry out complex tasks, despite the great variety of theoretical and practical challenges they pose. Within the different related topics in multirobot systems, there has been an increasing interest in target tracking problems [1].

A novel application of multirobot systems is the monitoring of a dynamic event. This application is highly related with optical motion capture systems (MOCAP) [2]. The goal of MOCAP, or motion tracking, is recording the movement of objects or people. Usually, the acquired information is used to animate digital models of human actors, where persistent full coverage of the surface and shape of the target is an essential requirement. In general, these systems consist of a set of fixed calibrated cameras around a certain space. Therefore, the actor is constrained to a limited workspace, with no flexibility to get out of this sensing *cage*.

Motivated by this application, consider that mobile robots with cameras on board are used instead of fixed cameras. This allows flexible configurations of the cameras around the target, with the possibility of handling occlusions. The cameras

could then follow the target without space limitations. For example, a set of robots could track a runner outdoors for miles to produce a 3D model at any time. In this work, we consider the target to be enclosed and tracked moves with unicycle kinematics. This suits the envisioned application since, in general, human locomotion can also be described by nonholonomic kinematics [3]. In order to complete the task, it is usual to assume that a global frame is available, using for instance a GPS system, or to require an external positioning system to reduce the uncertainty in estimating the agents’ poses [4], [5]. However, this type of systems is again restricted to limited setups (e.g. requiring GPS availability outdoor or a local positioning system indoor) and cannot be used to capture the dynamic target following long paths along different environments. This problem of motion coordination in the context of target tracking has been addressed in [6] by using consensus algorithms to perform flocking, or in [7] by filming a target through flying cameras.

Related to the tracking task, there is the problem of enclosing a target [8]. In general, this involves a team of robots maintaining a particular formation around the target. Usually, circular formations are considered for the enclosing task in 2D space [9], [10] or in 3D space [11], [12]. The task of circumnavigation around the target can also be included in the enclosing problem with the goal of monitoring the target by circling around it at a prescribed distance [13], [14]. This allows to deal with particular motions of the target such as pure rotations, which are not addressed in this paper. However, circumnavigation methods are typically free from the motion and visual constraints we consider here. They usually assume single integrator model [14], [15], impose more restricted bounds on the target motion (e.g. agents’ speeds required to be much more greater than the target speed, whereas here we consider same order of magnitude) [11], [16], [15], or do not consider controlling the headings of the agents. Managing simultaneously the shape of a formation and the headings of its agents [17], as we do here, is not usual in the literature. Related works to the task of enclosing are [16], where a distributed method based on local sensing is presented, and [14], [15], where distributed target enclosing is performed with a coordinate-free approach. Distributed gradient-based controllers to stabilize rigid formations were studied proving local asymptotic stability [18] or exponential convergence [19], [20]. A comprehensive survey of formation control of multi-agent systems can be found in [21].

In the task we address here, it is required not only to enclose

G. López-Nicolás is with Instituto de Investigación en Ingeniería de Aragón, Universidad de Zaragoza, Spain. gonlopez@unizar.es

M. Aranda and Y. Mezouar are with Université Clermont Auvergne, CNRS, SIGMA Clermont, Institut Pascal, F-63000 Clermont-Ferrand, France. first_name.last_name@sigma-clermont.fr

This work was supported by the French Government through the RobotEx Equipment of Excellence (ANR-10-EQPX-44), the IMobS3 Laboratory of Excellence (ANR-10-LABX-16-01) and the I-SITE project CAP 20-25, and by the Spanish Government/European Union through project PGC2018-098719-B-I00 (MCIU/AEI/FEDER, UE), and project COMMANDIA SOE2/P1/F0638 (Interreg Sudoe Programme, ERDF).

but also to monitor the target as it moves. Therefore, the goal is to provide the system with the ability of perceiving the target by means of multiple sensors (i.e. multiple robots) to obtain, e.g., a complete representation of this target. Vision sensors provide rich information while being widely available and relatively inexpensive, which has made them a usual choice in many robotic tasks. These features become particularly relevant when dealing with multi-robot systems. Existing approaches usually observe the target through vision sensors [5], [6], [7], [10].

A main drawback of standard cameras for the considered task is their limited field of view (FOV). This constraint is also hardened by the unicycle motion constraints considered. The problem of nonholonomic robot navigation while maintaining visibility of a fixed landmark using an onboard camera with a limited FOV was tackled in [22] and [23]. Optimality of the paths that are achieved was later addressed in [24], [25] and a visual servo control system based on homographies was also proposed in [26] by following optimal paths while taking care of the visual sensor constraints. These previous works model the camera FOV as a symmetric and planar cone aligned with the forward direction of motion. In [27], the synthesis of shortest paths with general FOV (e.g. side and lateral sensors) was provided. Time-optimality was also considered when addressing both nonholonomic and FOV constraints [28]. The problem of finding collision-free paths in an environment with obstacles with both nonholonomic and FOV constraints was tackled in [29].

These previous works consider only one robot and a static target to maintain in the FOV. The work presented in [30] addressed the problem of real-time trajectory generation in aerial videography with a single aerial vehicle that autonomously records scenes with moving targets optimizing for visibility. Regarding the multirobot approach, the control of multiple robots with limited FOV was studied for a containment task [31]. There, connectivity and consensus analysis were provided, although single-integrator robots are assumed and the goal is to converge to a static configuration, which prevents the application to a moving target. The work in [32] addressed the problem of cooperative coordination of leader-follower formations of mobile robots with visibility and communication constraints. The proposal in [32] aims at controlling a tractor-trailer formation in the presence of obstacles with forward-looking sensors rather than performing target perception.

Building on the previous work [33], we address the problem of enclosing and tracking a dynamic target with a team of robots while guaranteeing persistent full coverage of the surface and shape of the target along its motion. We consider a circular pattern configuration to enclose the target as shown in Fig. 1, but our framework allows flexibility to define the formation shape or the number of robots. For example, a critical application or hazardous environment may require to have redundancy in the sensing and the number of required enclosing robots could be increased. On the contrary, some applications could require perception of only a part of the target, allowing to reduce the number of robots to cover the area of interest. In the proposed system, the robots rely only on their onboard vision sensor without external input to complete

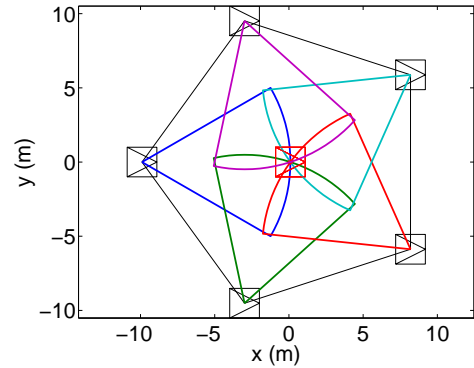


Fig. 1. Example of a desired formation with pentagonal shape in a circle of radius 10 m. The target to be observed is in the center of the formation. Each robot mounts a camera with a fixed orientation. The wedged shapes represent the angular limits of the camera FOV (visibility in distance is not constrained and the arc closing each wedge is just depicted for ease of the representation). The goal is to enclose and follow the target with the desired formation pattern while keeping both motion and FOV constraints.

the task. Notice that the fixed camera each robot carries is not necessarily forward-looking, but pointing in the direction as defined in the desired configuration.

Here, the key problem resides in overcoming the motion and visual constraints of the agents. In particular, the approach presented deals with three different issues. First, the desired geometric formation to enclose the target must be attained and maintained during the tracking. Second, the nonholonomic motion constraints of the enclosing robots must be taken into account by designing feasible reference formation trajectories. And third, visibility of the target must always be maintained by overcoming the limited field of view of the cameras. Addressing these three issues simultaneously represents an important challenge and, to the best of our knowledge, this is the first work dealing with them at the same time. In this scenario, we present a novel approach to characterize and analyze the conditions on the robots trajectories in order to comply with these motion and visual constraints. Taking into account this previous characterization, we also propose two online and two offline motion planning strategies to carry out the task of enclosing and tracking the target while addressing the constraints involved.

The presented approach provides a novel strategy that has the following advantages. The robots maintain a full representation of the target, which is also very stable in terms of sensing since the vantage angles are always maintained. For example, this quality is interesting to perform persistent monitoring of the entire target surface, which requires that every camera must always retain visibility of the target to avoid loss of coverage. The proposed strategy also guarantees that the robot motions are smooth, safe and comfortable for the target. Finally, the proposed strategy is also flexible in the sense that it is not limited to a particular formation shape.

Starting from the desired formation, we show that the desired task will be unfeasible in general. Then, we propose two different alternatives. On the one hand, we enforce maintaining the shape of the formation, but we allow variations in the scale, or the size, of this formation to guarantee existence

When the robots in the desired formation are evenly distributed around the target, the angles are denoted as θ_{0i} with coordinates x_{0i} and y_{0i} . In particular, we have

$$\theta_{0i} = \pi(2i/N - 1), \quad \text{with } i = 1, \dots, N. \quad (6)$$

In the following sections, we also consider several approaches regarding θ_i : The case of constant prescribed angles $\theta_i = \theta_{0i}$, evenly distributed as defined in (6), the general case with variable angles $\theta_i = \theta_{ri}(t)$, and the case of constant angles $\theta_i = \theta_{ci}$ to be defined by the proposed strategy guaranteeing existence of solution of the task.

Each robot in the formation has a camera on board, which is fixed on the robot and pointing to the target with a constant angle depending on θ_{0i} . In particular, in the circular formation considered for the enclosing task with all the robots equally oriented as depicted in Fig. 1, we have that for robot at θ_{0i} the camera forms a fixed angle of $(\theta_{0i} - \pi)$ if $\theta_{0i} > 0$, or $(\theta_{0i} + \pi)$ if $\theta_{0i} \leq 0$, with respect to its forward motion direction. In this nominal configuration, all the robots observe the target in the center of their FOV.

The FOV of each camera is limited by angle $\beta_i^{min} < 0$ and $\beta_i^{max} > 0$. For simplicity, we assume symmetric FOV ($\beta_i = -\beta_i^{min} = \beta_i^{max}$) and that all the cameras have the same FOV ($\beta_i = \beta$). For each robot, maintaining the target in its field of view implies keeping the projection of target $\beta_{ti}(t)$ in robot's camera i such that $\beta_{ti} \in [-\beta, \beta]$.

Considering the framework described in the previous paragraphs, we next define the problem to be addressed.

Problem definition: *Given a unicycle-type moving target (1) and a team of unicycle-type robots (2) enclosing that target in circular formation, find an appropriate strategy for the robots' trajectories to maintain the shape (varying d strategy) or the size (varying θ_i strategy) of the formation, while guaranteeing that the target is always in the field of view of all onboard cameras, i.e. $\beta_{ti} \in [-\beta, \beta]$.*

An illustration of this problem with an example is provided in Fig. 3. In this example, the target follows an ellipsoidal motion enclosed by five robots that form a regular pentagon. Robot trajectories are defined so as to maintain a rigid formation with $d_i = d_0 = 5m$ without enforcing FOV constraints. Although the robot formation is always maintained, the target leaves the FOV of some robots during the sharper curves of the motion. This can also be seen in the FOV plot around $t = 50s$ and $t = 150s$, where the projection of the target in some robots' cameras goes beyond the FOV limits, which have been defined as $\beta = 30deg$. The velocities of the target (v_t, ω_t) and the robots (v_{ri}, ω_{ri}), whose computation is presented in the next section, are also shown in Fig. 3. In general, the closer the robots' velocities to the target velocity, the easier it becomes to respect FOV constraints. The angular velocity plot of ω_{ri} shows the sharper turns that allow maintaining the formation but also causing the break of the FOV constraint. Notice that the effect of changing the scale of the formation may seem counter-intuitive. One may expect that the bigger the formation size, the easier it is to keep the target in the FOV. However, reality shows that as the distance between the robot and the target grows, sharper velocities will be required

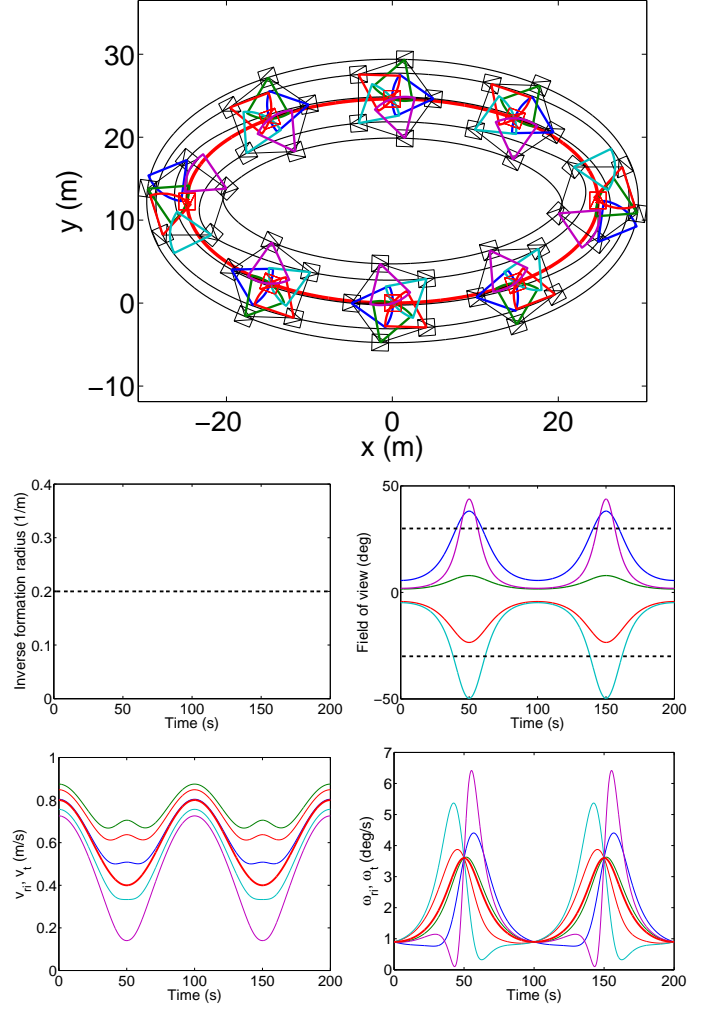


Fig. 3. Example of enclosing and tracking a target with ellipsoidal motion. Formation is compounded by 5 robots forming a pentagon with constant scale $d_0 = 5m$ without considering FOV constraints. Top: motion of the robots. Second row: Inverse radius $\kappa_0 = 1/d_0$ (left), and angle of the target in the FOV of each camera β_{ti} (right). Bottom: velocities (v_{ri}, ω_{ri}) of all the robots and the target (v_t, ω_t) (thicker line).

to track the target within the formation, and sharper motions may lead to the FOV constraint break.

The next example in Fig. 4 shows the influence of the formation scale in keeping the target within the FOV limits of the cameras. We repeat the simulation of Fig. 3 with different values of the formation scale $d_0 \in (0, 80]m$. For each simulation and over a complete ellipsoidal path, we compute the time each robot kept the target in its FOV and depict this value in percentage. It is clear that increasing the scale of the formation leads to lower time percentages of maintenance of the target in the FOV of the robots' cameras. Notice that depending on the robot location in the formation (θ_i) the results are quite different. See for instance that one of the robots always maintains the target in its FOV limits (100%), this is the robot located in $\theta_2 = -108deg$. In the opposite situation is the robot located in $\theta_4 = 36deg$, which is the first in reaching 0% when increasing the formation scale. This means that higher scales results in the computation of sharper curves in the reference trajectories that may lead to the total

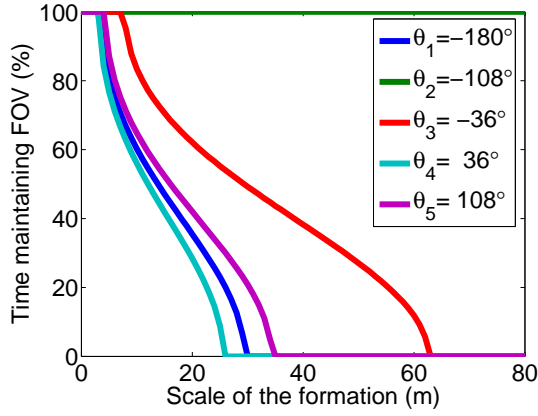


Fig. 4. Example illustrating the effect of the scale of the formation (d_0) in keeping the FOV constraints. For the example of enclosing and tracking a target with ellipsoidal motion (Fig. 3), different values of d_0 are tested. For each d_0 , we measure the percentage of time each robot keeps the target in its field of view. With low d_0 all of them hold FOV constraints all the time (i.e. 100%) whereas using higher d_0 reduces this percentage depending on the robot location in the formation until reaching total loss of the FOV.

loss of the FOV. Since we do not assume the target is initially in the FOV of the cameras, the 0% value can be found at initial time in this example. Hereafter, we assume that the initial configuration is the desired one and preliminary manoeuvres are not required before starting the task. Then, the problem to solve is to track the target maintaining this formation while taking into account the constraints.

III. CONSTRAINTS ON REFERENCE FORMATION TRAJECTORIES

In this section, we present the different constraints on the robots' reference trajectories to enclose and track the moving target in rigid shape formation while taking into account the motion and visibility limits.

The problem of finding appropriate trajectories to be tracked by the robots of the formation while keeping the formation shape geometry as well as motion and visibility constraints is defined as the problem of finding a suitable reference trajectory for each robot. These trajectories are defined for each robot by its position $\mathbf{q}_{ri}(t) = (x_{ri}(t), y_{ri}(t))^T$ and orientation $\phi_{ri}(t) \in \mathcal{R}$, with $i = 1, \dots, N$. In order to create feasible trajectories we impose unicycle kinematics

$$\begin{pmatrix} \dot{x}_{ri} \\ \dot{y}_{ri} \\ \dot{\phi}_{ri} \end{pmatrix} = v_{ri} \begin{pmatrix} \cos \phi_{ri} \\ \sin \phi_{ri} \\ 0 \end{pmatrix} + \begin{pmatrix} 0 \\ 0 \\ \omega_{ri} \end{pmatrix}, \quad (7)$$

where $v_{ri}(t) \in \mathcal{R}$ and $\omega_{ri}(t) \in \mathcal{R}$ are the linear and angular velocities that generate the reference trajectories to be tracked by the robots.

For given target velocities v_t and ω_t or equivalently, the target path (x_t, y_t) and ϕ_t , we express the coordinates of each robot (5) with respect to the global reference frame

$$\begin{pmatrix} x_{ri} \\ y_{ri} \end{pmatrix} = \begin{bmatrix} \cos \phi_t & -\sin \phi_t \\ \sin \phi_t & \cos \phi_t \end{bmatrix} \begin{pmatrix} x_i \\ y_i \end{pmatrix} + \begin{pmatrix} x_t \\ y_t \end{pmatrix}, \quad (8)$$

which reduces to

$$\begin{pmatrix} x_{ri} \\ y_{ri} \end{pmatrix} = \begin{pmatrix} x_t \\ y_t \end{pmatrix} + d \begin{pmatrix} \cos(\phi_t + \theta_i) \\ \sin(\phi_t + \theta_i) \end{pmatrix}, \quad (9)$$

where $d = d_i$ is the common scale as defined in (3). So, if the N robots follow the trajectories x_{ri} and y_{ri} , their positions satisfy the desired formation geometry with respect to the target. Calculating the time derivative of this vector yields

$$\begin{aligned} \dot{x}_{ri} &= v_t \cos \phi_t - d(\omega_t + \dot{\theta}_i) \sin(\phi_t + \theta_i) + \dot{d} \cos(\phi_t + \theta_i), \\ \dot{y}_{ri} &= v_t \sin \phi_t + d(\omega_t + \dot{\theta}_i) \cos(\phi_t + \theta_i) + \dot{d} \sin(\phi_t + \theta_i). \end{aligned} \quad (10)$$

The reference orientation ϕ_{ri} is then obtained as follows

$$\tan \phi_{ri} = \dot{y}_{ri} / \dot{x}_{ri}. \quad (11)$$

The velocities v_{ri} and ω_{ri} can be expressed from (7), (10) and derivative of (11) as $v_{ri}^2 = (\dot{x}_{ri})^2 + (\dot{y}_{ri})^2$ and $\omega_{ri} = \dot{\phi}_{ri} = \cos^2 \phi_{ri} (\dot{x}_{ri} \dot{y}_{ri} - \ddot{x}_{ri} \dot{y}_{ri}) / (\dot{x}_{ri})^2$. Then, the forward velocity for each robot is computed from (7) and (10) as follows

$$\begin{aligned} v_{ri}^2 &= d^2 (\omega_t + \dot{\theta}_i)^2 + \dot{d}^2 + v_t^2 \\ &+ 2 v_t \left(\dot{d} \cos \theta_i - d (\omega_t + \dot{\theta}_i) \sin \theta_i \right). \end{aligned} \quad (12)$$

On the other hand, the angular velocity from (7) and the time derivative of (11) yield

$$\begin{aligned} \omega_{ri} &= \omega_t + d^2 \dot{\theta}_i (\omega_t + \dot{\theta}_i)^2 / v_{ri}^2 \\ &+ (\dot{d}^2 + d \dot{d} \dot{\omega}_t - d \ddot{d}) \omega_t / v_{ri}^2 \\ &+ \left(\ddot{d} v_t - \dot{d} \dot{v}_t - d v_t \dot{\theta}_i (\omega_t + \dot{\theta}_i) \right) \sin \theta_i / v_{ri}^2 \\ &+ d \left(v_t (\dot{\omega}_t + \ddot{\theta}_i) - \dot{v}_t (\omega_t + \dot{\theta}_i) \right) \cos \theta_i / v_{ri}^2 \\ &+ (\dot{d} v_t \omega_t - d \dot{v}_t \omega_t + d v_t \dot{\omega}_t) \cos \theta_i / v_{ri}^2. \end{aligned} \quad (13)$$

In order to define the particular velocities required to follow the reference formation trajectories, we consider in the following proposition the general case in which both d and θ_i are allowed to vary. Then we consider the particular cases in which only d or θ_i is allowed to vary to fulfill the different constraints. Finally, we present the cases in which either d or θ_i is set to a constant value, d_c or θ_{ci} respectively, to be determined with the proposed strategy.

Proposition 1: Field of view constraints with variable scale and variable formation angles. The constraint that guarantees that FOV limits are respected when letting $d_i(t)$ and $\theta_i(t)$ vary is the following

$$\left| \frac{v_t \sin \theta_i - d_i (\omega_t + \dot{\theta}_i)}{d_i + v_t \cos \theta_i} \right| \leq |\tan(\theta_{0i} \pm \beta)|, \quad i = 1, \dots, N.$$

Proof:

The velocities deduced in (12) and (13) allow tracking the target with variable scale and formation angles but, since no FOV constraint has been imposed yet, there is still no guarantee of maintaining the moving target in the cameras' FOV. Next we proceed to obtain the analytical expression of the field of view constraint. First, we introduce (10) in (11) removing explicit dependency on \dot{x}_{ri} and \dot{y}_{ri} obtaining the following equation

$$d_i (\omega_t + \dot{\theta}_i) - \dot{d}_i \tan(\phi_{ri} - \phi_t - \theta_i) = \frac{v_t \sin(\phi_{ri} - \phi_t)}{\cos(\phi_{ri} - \phi_t - \theta_i)}. \quad (14)$$

Now, we look for the visual constraint on the relative angle between each robot and the target. This relative angle plus the

threshold provided by the limiting angle β of the FOV gives the maximum orientation to maintain the target in the FOV of each robot. In particular, this implies $-\beta \leq \phi_t - \phi_{ri} + \theta_i - \theta_{0i} \leq \beta$. Therefore, denoting $\beta_{ri}(t) = \phi_t - \phi_{ri} + \theta_i - \theta_{0i}$ in (14), and $\beta_{ti} = \beta_{ri}$, we obtain

$$\phi_{ri} - \phi_t = \theta_i - \theta_{0i} - \beta_{ri}. \quad (15)$$

Then, using (15) in (14) and solving for $(\theta_{0i} + \beta_{ri})$ gives the following constraint

$$|\tan(\theta_{0i} + \beta_{ri})| \leq |\tan(\theta_{0i} \pm \beta)|, \quad (16)$$

with

$$\tan(\theta_{0i} + \beta_{ri}) = \frac{v_t \sin \theta_i - d_i (\omega_t + \dot{\theta}_i)}{\dot{d}_i + v_t \cos \theta_i}. \quad (17)$$

Case 1: Field of view constraints with variable scale.

In this case, in order to respect FOV constraints we allow the scale of the formation to change during the motion, $d_i = d_r(t)$, whereas $\theta_i = \theta_{0i}$ are kept constant. Then, the forward and angular velocities for each robot are computed from (12) and (13), and the FOV constraint is deduced from (16) and (17). Then, solving for β_{ri} yields the following constraint

$$-\tan \beta \leq \tan \beta_{ri} \leq \tan \beta \quad (i = 1, \dots, N) \quad (18)$$

which needs to hold for every robot, with

$$\tan \beta_{ri} = \frac{d_r \omega_t \cos \theta_{0i} + \dot{d}_r \sin \theta_{0i}}{d_r \omega_t \sin \theta_{0i} - \dot{d}_r \cos \theta_{0i} - v_t}. \quad (19)$$

Then, the constraint that guarantees that FOV limits are respected when letting $d_i = d_r(t)$ vary, while using the prescribed fixed angles $\theta_i = \theta_{0i}$, is the following

$$\left| \frac{d_r \omega_t \cos \theta_{0i} + \dot{d}_r \sin \theta_{0i}}{d_r \omega_t \sin \theta_{0i} - \dot{d}_r \cos \theta_{0i} - v_t} \right| \leq \tan \beta, \quad i = 1, \dots, N.$$

Case 2: Field of view constraints with constant formation scale.

This is a particular case of *Case 1* when considering a constant value of the formation scale ($d_i = d_c$) instead of a variable one, while again $\theta_i = \theta_{0i}$ is constant. Analytical expression of the field of view constraint in this case is obtained from (14) with $\dot{d}_i = 0$ and $\theta_i = \theta_{0i}$. Taking into account the FOV constraint $|\phi_t - \phi_{ri}| \leq \beta$ and (4) yields the following limit constraint

$$d_c = \frac{1}{\kappa_c} \leq d_i = \frac{1}{\kappa_i} = \left| \frac{v_t \sin(\pm\beta)}{\omega_t \cos(\pm\beta - \theta_{0i})} \right|. \quad (20)$$

Let us denote the worst case of κ_i for all i with

$$\kappa_{wc}(t) = \max_i(\kappa_i). \quad (21)$$

We also define the maximum value of κ_{wc} as

$$\kappa_L = \max_t(\kappa_{wc}) = \max_t \left| \frac{\omega_t}{v_t \sin(\pm\beta)} \right|, \quad (22)$$

which is found when θ_{0i} takes any of these values:

$$\theta_{0i} = \{\pm\beta, \pm\beta - \pi\}. \quad (23)$$

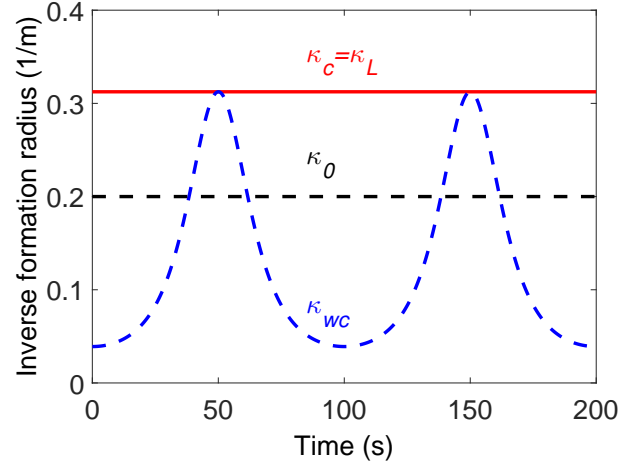


Fig. 5. Evolution of $\kappa = 1/d$ for example in Fig. 3. The lower varying dashed line corresponds to the limit κ_{wc} (18). Any value below this limit violates the FOV constraint. Horizontal dashed line corresponds to the scale used in the simulation: $d_0 = 5 \text{ m}$ ($\kappa_0 = 0.2 \text{ m}^{-1}$). It can be seen that around $t = 50 \text{ s}$ and $t = 150 \text{ s}$ the FOV constraint is violated. The closest constant value that guarantees FOV constraint corresponds with the top horizontal solid line at $\kappa_c = 0.31 \text{ m}^{-1}$ ($d_c = 3.2 \text{ m}$) given by (22).

Then, the constraint that guarantees that FOV limits are respected when imposing a constant $d_i = d_c$ to be defined ($i = 1, \dots, N$), while using the prescribed fixed angles $\theta_i = \theta_{0i}$, is the following:

$$d_c \leq 1/\kappa_L = 1/\max|\omega_t/(v_t \sin(\pm\beta))|. \quad (24)$$

Any constant value $\kappa_c < \kappa_L$ will violate FOV limits. Therefore, choosing $\kappa_c = \kappa_L$ to define the inverse scale of the formation guarantees that the target is always maintained in the FOV. Notice that the computation of the limit value κ_L , and consequently the maximum radius of the formation, involves the maximum curvature of the target's trajectory $\kappa_{t_{max}}$, whose knowledge is thus needed in advance.

Following the example of Fig. 3, we illustrate the scale constraints in Fig. 5. The evolution of the inverse formation radius is plotted in three cases: κ_{wc} by using FOV constraint (18) in the worst case (21), i.e. with (23); κ_L by using the constant value computed with (22); and using an arbitrary prescribed value $\kappa_0 = 1/d_0$ that violates the FOV constraint. Notice that the higher the value above κ_c is, the closer to the target the robots of the formation are. This eases the FOV problem but practical considerations will require a safety distance (in the limit $\kappa_c \rightarrow \infty$ the robots overlap with the target, i.e. $d_c = 0$).

In the previous cases, we let d_r vary along time or we define a constant value d_c . However, in some applications the scale of the formation may be defined in advance with the requirement of keeping it fixed (for example to keep a safety distance with the target). Then, we may consider some flexibility on the shape of the formation allowing variations of θ_i with respect to θ_{0i} . Following this idea we present the next case.

Case 3: Field of view constraints with variable formation angles.

In this case, the forward and angular velocities for each robot are computed from (12) and (13) with $d_i = d_0$ constant and

$\theta_i = \theta_{ri}(t)$ variable. These velocities guarantee that the robots follows θ_{ri} and maintain the prescribed formation scale around the target during the tracking, but there is still not guarantee of maintaining the moving target in the cameras' FOV. The analytical expression of the FOV constraint is defined from (17) with $\dot{d}_i = 0$. This gives the following constraint

$$|\tan(\theta_{0i} + \beta_{ri})| = \left| \tan \theta_{ri} - \frac{d_0 (\omega_t + \dot{\theta}_{ri})}{v_t \cos \theta_{ri}} \right| \leq |\tan(\theta_{0i} \pm \beta)|. \quad (25)$$

Finally, solving for β_{ri} results in

$$|\beta_{ri}| = \left| \arctan \left(\frac{v_t \sin \theta_{ri} - d_0 (\omega_t + \dot{\theta}_{ri})}{v_t \cos \theta_{ri}} \right) - \theta_{0i} \right| \leq \beta, \quad (26)$$

which is the constraint that guarantees that FOV limits are respected when imposing a prescribed constant $d_i = d_0$ and letting $\theta_i = \theta_{ri}(t)$ vary. In this case, we let θ_{ri} vary along time to overcome the situation in which the prescribed angles of the desired formation θ_{0i} violate the problem constraints. In the next case, we define a set of constant angles θ_{ci} that, unlike the prescribed formation angles θ_{0i} , respect the different constraints of the problem.

Case 4: Field of view constraints with constant formation angles.

This is a particular case of *Case 3* considering constant values of the formation angles θ_{ci} that can be different from the prescribed angles θ_{0i} of the desired formation. Considering $\theta_i = \theta_{ci}$ to be defined with a constant value for each robot i , and $d_i = d_0$ also constant (with a previously given value), after some development and taking into account FOV constraint $|\phi_t - \phi_{ri} + \theta_{ci} - \theta_{0i}| \leq \beta$ and considering both limit values $\pm\beta$, we obtain from (14)

$$\sin \theta_{ci} - \tan(\theta_{0i} \pm \beta) \cos \theta_{ci} = d_0 \omega_t / v_t. \quad (27)$$

Then, the constraint that guarantees that FOV limits are respected when imposing a prescribed constant $d_i = d_0$, and letting $\theta_i = \theta_{ci}$ to be defined using constant values, is

$$\theta_{ci} \in [\underline{\theta}_i, \bar{\theta}_i], \quad \forall i, \quad (28)$$

where $\underline{\theta}_i$ and $\bar{\theta}_i$ are given by $\text{atan2}(1, -\tan \theta_\beta) \mp \arccos(d_0 \omega_t \cos(\theta_\beta) / v_t)$ with $\theta_\beta = (\theta_{0i} \pm \beta - \pi)$ if $(\pi/2 \mp \beta) < \theta_{0i} < (-\pi/2 \mp \beta)$, and $\theta_\beta = (\theta_{0i} \pm \beta)$ otherwise.

Equation (27) yields the interval of $\theta_{ci} \in [-\pi, \pi]$ defined in the constraint with $\underline{\theta}_i$ the lower bound along time and $\bar{\theta}_i$ the upper bound. Notice that there are two possible solutions of $\underline{\theta}_i$ and $\bar{\theta}_i$ so the correct pair is selected by checking the smallest interval $[\underline{\theta}_i, \bar{\theta}_i]$ solution around θ_{0i} . Notice also that the FOV constraint in (28) depends on the value of θ_{0i} . Then, the values of θ_{0i} given in (23) refer to the worst case for the FOV constraint in the sense that they make the interval of the constraint $[\underline{\theta}_i, \bar{\theta}_i]$ smaller. Then, $\theta_{ci} \in [\underline{\theta}_i, \bar{\theta}_i]$ is a necessary condition to satisfy FOV constraints.

Considering again the example in Fig. 3, the latter constraints on the angles θ_{ci} are illustrated in Fig. 6. The evolution of the lower $\underline{\theta}_i$ and upper $\bar{\theta}_i$ bounds (28) are plotted for each robot showing the intervals that constrain the values of θ_{ci} to guarantee visibility of the target. The constant values of θ_{0i}

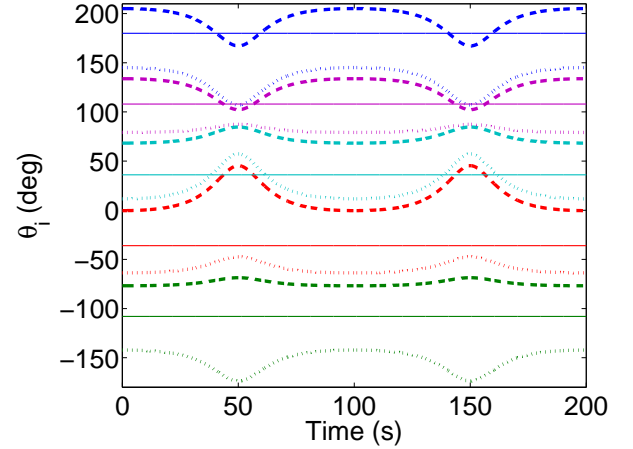


Fig. 6. Evolution of the FOV constraints defined for θ_{ri} in *Case 4* using example in Fig. 3. For each robot (a different color per robot), the upper bound of the constraint $\bar{\theta}_i$ is plotted in dashed line, the lower bound $\underline{\theta}_i$ is plotted in dotted line, and the actual value used in the simulation θ_{0i} is plotted in solid line (better seen in color). Around $t = 50$ s and $t = 150$ s some of the robots go beyond the bounds breaking the FOV constraint.

are also plotted showing that two of the robots respect the FOV constraint (with values -108 deg and -36 deg) whereas the rest of the robots lose visibility of the target at some times. Note that if variable θ_{ri} is considered, the designed value of θ_{ri} not only must be inside the interval defined by (28) but also must obey constraint (26).

Remark 1: Indeterminate terms.

Notice that there can be indeterminate terms of the form $0/0$ in the computation of ω_{ri} in (13) for some i when $v_{ri} = 0$. The indeterminate term appears in the different *Cases 1* to *4* when any of the following two sets of conditions holds:

$$d_i (\omega_t + \dot{\theta}_i) = v_t \sin \theta_i \quad \wedge \quad \dot{d}_i = -v_t \cos \theta_i, \quad (29)$$

$$d_i \omega_t = \pm v_t \quad \wedge \quad \theta_i = \pm \pi/2 \quad \wedge \quad \dot{d}_i = 0, \quad (30)$$

or also in the trivial case

$$v_t = 0 \quad \wedge \quad (\omega_t + \dot{\theta}_i) = 0 \quad \wedge \quad \dot{d}_i = 0. \quad (31)$$

In all the previous cases, the indeterminate terms tend to zero and then $\omega_{ri} = \omega_t$. All these indeterminate terms come from the following cases. On the one hand, the indeterminate form appears with null velocities of the robots and the target. On the other hand, the indeterminate form appears when the target rotates around robot i , requiring a pure rotation of the robot i reference trajectory. The problem of these indeterminate terms can be easily avoided if the target trajectory curvature is bounded (*Assumption 1*), such that $\kappa_{t_{max}} < 1/d_i$.

Remark 2: Existence of solution. Given a desired shape formation, *Cases 1* and *2*, in which the scale of the formation is set to maintain FOV constraints, are guaranteed to have solution (i.e., we can find a motion strategy that guarantees FOV). This is trivial from (22) where, given β and a bounded value of ω_t/v_t , the value of κ_L can be directly found.

Regarding the existence of solution when the scale is not allowed to change, and only the values of θ_i can be modified (*Cases 3* and *4*), we have that existence of solution is not

guaranteed. In particular, the solution provided in *Case 4* only exists when the following condition holds

$$v_t^2 \geq d_0^2 \omega_t^2 \cos^2(\theta_{0i} \pm \beta), \quad (32)$$

Otherwise, there is no value of θ_{ci} to satisfy the FOV constraints. In that case, it would be necessary to modify the parameters of the problem: Increase β , reduce d_0 , or limit the target path curvature κ_t .

IV. STRATEGIES FOR REFERENCE FORMATION TRAJECTORIES

In the previous section, the constraints that allow to keep the target within the camera FOV limits have been presented. In the following, we propose several strategies to define particular reference trajectories that are compliant with these constraints, the unicycle motion constraints, and the maintenance of the formation pattern.

The scale of the formation d_i and its derivative \dot{d}_i (angles θ_i and $\dot{\theta}_i$ alternatively) give the degrees of freedom needed to define an appropriate reference tracking trajectory to guarantee keeping both motion and FOV constraints. However, it is important to notice that both constraints must be checked because obeying any of them does not guarantee obeying the other. In particular, one could define an arbitrary strategy to choose the value of d_i (the same for all i) satisfying (18), but we need also to check if d_i allows to follow the unicycle kinematics (9) and (11). Otherwise, the defined value of d_i may be incompatible with some constraints (unless the strategy is to assign a constant value to d_i , or θ_i , obeying FOV constraint, which trivially also holds motion constraints). Similarly, one could define an arbitrary strategy to choose the value of d_i satisfying unicycle kinematics, (9) and (11), but obviously this does not guarantee maintaining FOV constraints and therefore (18) needs to be checked. Once the appropriate strategies give the values of d_i (or θ_i) to fulfill simultaneously all the constraints, the robots' velocities can be directly computed from (12) and (13).

Four different strategies are presented in the next sections by defining an appropriate constant formation scale or constant formation angles, and variable formation scale or variable formation angles.

A. Constant formation scale: $d_i = d_c$ and $\theta_i = \theta_{0i}$

In order to fulfill the FOV constraint, we let the scale of the enclosing formation as a free parameter while the shape of the formation is enforced to be fixed. Then, the simplest strategy is to define the scale of the formation with the limit value of the FOV constraint for the full target trajectory. As previously commented the constant formation scale strategy is also guaranteed to respect the motion constraints of the robots. In particular, a constant scale of the formation is defined as computed in (22), (*Case 2*):

$$d_c = 1/\kappa_L. \quad (33)$$

By doing so, we maximize the scale of the formation with a constant value from constraint $d_c \leq 1/\kappa_L$. This choice is illustrated in Fig. 5 where the selected κ_L is always above κ_{wc}

guaranteeing maintenance of FOV constraints. Notice that any smaller scale will also guarantee the FOV constraint, whereas a higher constant value of d_c (such as d_0 , i.e. κ_0 , in the example) will violate this constraint some time.

In the example provided in Fig. 3, in which the target follows an ellipsoidal motion and the robots form a regular pentagon with $\beta = 30 \text{ deg.}$, no strategy is applied and the vision constraint is violated during the motion when the target leaves the FOV of some cameras. Following this example, we now present the result of using the presented constant formation scale strategy with $d_c = 3.2 \text{ m}$ to obey the constraints in Fig. 7 (top-left, and second row). This is the simplest strategy that guarantees maintaining the dynamic target in the FOV of the cameras. It can be noticed that the higher the curvature of the target's motion (κ_t), the smaller the value of d_c has to be in order to keep FOV constraints. This means that sharp motions of the target imply sharp reactions of the robots. That is to say, for a given β , smaller scale in the formation allows more leeway for keeping the FOV during the enclosing motion and hence allowing for sharper motions of the target. On the other hand, when the value of κ_t is low, the minimum required scale of the formation can be higher. For example, a particular case is when the target follows a straight line, in that case the scale of the formation could be arbitrarily high.

B. Variable formation scale: $d_i = d_r(t)$ and $\theta_i = \theta_{0i}$

The strategy proposed in the previous section is based on a constant value of the formation scale. This value d_c is the maximum without violating the FOV constraints when the target is turning with its maximum curvature $\kappa_{t_{max}}$. Nevertheless, d_c can still be increased when $\kappa_t < \kappa_{t_{max}}$ while maintaining FOV constraints (*Case 1*). In fact, any reference trajectory (9), (11) with corresponding velocities (12) and (13), that obeys the constraint in (18), and follows an appropriate strategy for d_r (and \dot{d}_r) is a suitable solution of the enclosing and tracking problem considered.

The next strategy we propose is based on maximising the distance between the enclosing robots and the target. This strategy can be useful for example to increase the safety distance between robots to prevent collisions.

We will define the reference evolution of κ , denoted κ_r . In order to do so, we set a constant upper bound given by κ_L (22), and a lower bound provided by κ_{wc} (18). Thus, any valid reference trajectory is constrained between κ_L , which is limiting the scale of the formation when the curvature of the target trajectory is maximum, and the value given by κ_{wc} , which gives the scale that reaches the FOV limits.

Any function of differentiability class C^2 or higher and with enough degrees of freedom could be used to define κ_r . For instance, typical choices that will result in similar performance can be polynomial, sinusoidal, or exponential functions. Since there are many possible choices, we look for smooth simple functions that can be defined with few parameters such that the involved computations can be more efficient. Inspired by the optimal paths presented in [24], which consisted in exponential

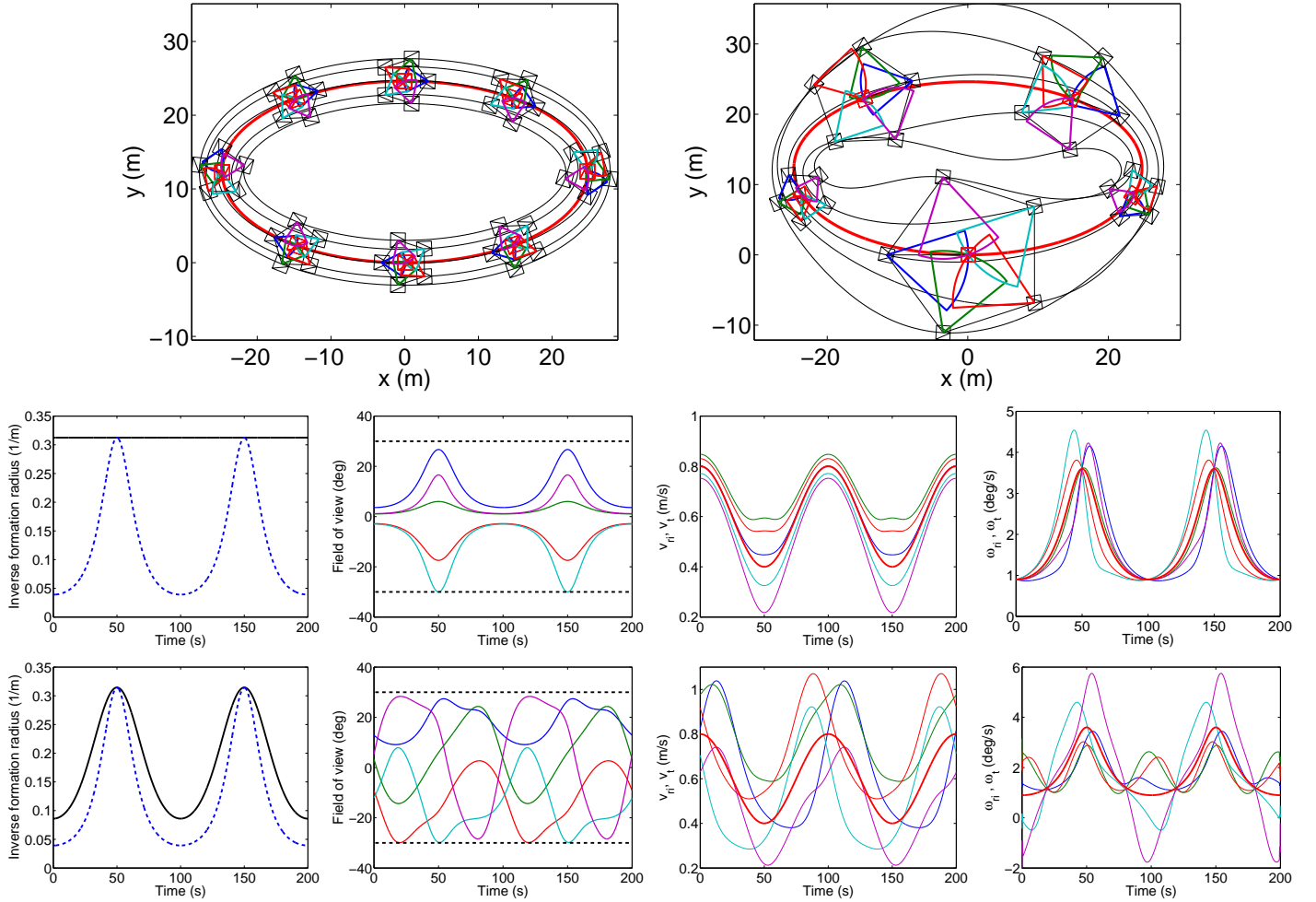


Fig. 7. Example of Fig. 3 using constant scale formation strategy presented in Section IV-A (top-left and second row) and variable formation scale strategy presented in Section IV-B (top-right and third row). Top: motion of the robots. Second and third row, from left to right: evolution of κ ; projection angle of the target in the FOV of each camera β_{ti} ; linear velocities v_{ri} of all the robots and the target v_t ; and angular velocities ω_{ri} of all the robots and the target ω_t . Target velocities are in thicker line. In the first strategy (22), we draw in solid line the selected constant value of $\kappa_L = 0.31 \text{ m}^{-1}$ ($d_c = 3.2 \text{ m}$). Respectively in the second strategy, the selected varying value κ_r is given by (34). Both strategies obey the FOV constraint κ_{wc} (18), in dashed line.

functions, we propose to use Gaussian type functions to define κ_r (with $d_r = 1/\kappa_r$):

$$\kappa_r = \kappa_L + \sum_{b=t_\delta} a (\kappa_{wc} - \kappa_L) \circ \exp\left(-\left(\frac{t-b}{c\sqrt{2}}\right)^2\right), \quad (34)$$

with “ \circ ” the Schur product (or entry-wise product). This function is defined in the time interval $t \in (t_i, t_f)$ where the target motion occurs. Parameter t_δ is defined as the sampled time with N_δ the number of samples between t_i and t_f :

$$t_\delta = t_i + \delta (t_f - t_i) / N_\delta, \quad \text{with } \delta = 0, \dots, N_\delta. \quad (35)$$

The value of κ_{wc} over time is computed from (18) with $\dot{d}_r = 0$ as shown in Fig 5. Parameters a and c are real constants to be found with the following optimization

$$\arg \max_{a,c} \int_{t_i}^{t_f} (\kappa_L - \kappa_r) dt, \quad (36)$$

subject to: $a, c \in \mathcal{R}^+$, $|\beta_{ri}| \leq \beta$.

The goal of this optimization is to find the values of a and c that bring κ_r closer to the constraint limits (18) without

violating formation and motion constraints (i.e., to maximize the area between κ_r and the value of κ_L). Notice that $\kappa_r = \kappa_{wc}$ is not a valid option since κ_{wc} does not comply with motion constraints (the orientation is decoupled from the motion).

This variable formation scale strategy is illustrated in Fig. 7 (top-right, and third row) in which the target follows an ellipsoidal motion and the robots form a regular pentagon with $\beta = 30 \text{ deg}$. The difference between this strategy (varying κ_r) and the previous one in Section IV-A ($\kappa_L = 0.31 \text{ m}^{-1}$) can be clearly seen in the left plots in second and third row of Fig. 7, where the solid line represents the proposed evolution of κ_L and κ_r , and the dashed line is the FOV limit (18).

C. Constant formation angles: $d_i = d_0$ and $\theta_i = \theta_{ci}$

Previous strategies in Sections IV-A and IV-B maintain the formation shape but assuming its scale $d_i = d_c$ can be adapted. However, some applications may require a particular prescribed fixed scale $d = d_0$ to maintain, for instance, this particular distance between the robots and the target for safety

or accuracy reasons. Here, we propose a different strategy in which the robots are allowed to modify their relative position in the formation while keeping the prescribed constant distance with the target.

Next we search for constant values of θ_{ci} such that FOV constraints are guaranteed with the limits presented in *Case 4*. If we already have the prescribed values $\theta_{0i} \in [\underline{\theta}_i, \bar{\theta}_i]$ for some i , then there is no need to define other value for θ_{0i} since FOV constraints will be respected by robot i . Otherwise, we choose a value between the global minimum and maximum values of the bounds as follows

$$\theta_{ci} = \begin{cases} \theta_{ci}^{min} & \text{if } \theta_{0i} < \theta_{ci}^{min} \\ \theta_{ci}^{max} & \text{if } \theta_{0i} > \theta_{ci}^{max} \\ \theta_{0i} & \text{if } \theta_{ci}^{min} \leq \theta_{0i} \leq \theta_{ci}^{max} \end{cases} \quad (37)$$

for $i = 1, \dots, N$, and where the global minimum and maximum values are defined as

$$\theta_{ci}^{min} = \max_t(\underline{\theta}_i), \quad \theta_{ci}^{max} = \min_t(\bar{\theta}_i), \quad i = 1, \dots, N. \quad (38)$$

Any constant value inside the range in (28) will be valid to hold FOV constraints. Here, we choose for θ_{ci} the closest constant value to the prescribed formation values θ_{0i} . Then, we are deforming the prescribed formation as little as possible. Note that there is no guarantee that a solution exists for choosing a constant value for θ_{ci} (*Remark 2*). The more contorted the target trajectory is, the fewer chances to find a solution. If no solution is found, but the application still requires constant values θ_{ci} , then the target motion should be limited ($\kappa_{t_{max}}$) or the system parameters modified (scale d_0 of the formation or cameras FOV β).

Following again the example provided in previous figures in which the target follows an ellipsoidal motion and the robots form a regular pentagon with $\beta = 30 \text{ deg.}$, we present the result of using this constant formation angles strategy, with $\theta_{ci} = (-108.00, -36.00, 57.36, 102.29, 167.14) \text{ deg.}$ in Fig. 8 (top-left, and second row). It can be seen that the formation is no longer a regular pentagon, but the scale of the formation (distance of each robot to the target $d_0 = 5 \text{ m}$) is kept fixed as pointed out with the plotted circle.

D. Variable formation angles: $d_i = d_0$ and $\theta_i = \theta_{ri}(t)$

Instead of just using constant values for θ_i to respect the problem constraints, we propose another strategy in which the reference values of θ_{ri} are allowed to vary with time. Then, they will only need to be modified when the constraints are violated with the predefined values of θ_{0i} . This strategy preserves the desired formation shape when possible by only adapting it to keep the FOV constraints when necessary.

Given the lower bound $\underline{\theta}_i$ and upper bound $\bar{\theta}_i$ of θ_i to obey FOV constraints (*Case 4*), we need to define smooth functions for these angles such that $\theta_i \in [\underline{\theta}_i, \bar{\theta}_i]$ for all times. The evolution of the values to be defined for θ_i not only must be within the bounds (28) but their derivative must also not violate constraint (25). The FOV constraint is violated for any t in which $\theta_i > \bar{\theta}_i$ or $\theta_i < \underline{\theta}_i$. In order to define the reference evolution θ_{ri} , if the constraint is respected, we keep

the predefined value θ_{0i} . Otherwise, we define a function θ_{gi} to compute θ_{ri} :

$$\theta_{ri} = \begin{cases} \theta_{gi} & \text{if } \theta_{0i} > \theta_{ci}^{max} \text{ or } \theta_{0i} < \theta_{ci}^{min} \\ \theta_{0i} & \text{if } \theta_{ci}^{min} \leq \theta_{0i} \leq \theta_{ci}^{max} \end{cases} \quad (39)$$

for $i = 1, \dots, N$. The global minimum and maximum values along time are defined as in (38). Similarly to the strategy in Section IV-B, we use Gaussian type functions to define θ_{gi} :

$$\theta_{gi} = \theta_{0i} + \sum_{b=t_\delta} a(\bar{\theta}_{xi} + \underline{\theta}_{xi}) \circ \exp\left(-\left(\frac{t-b}{c\sqrt{2}}\right)^2\right), \quad (40)$$

with “ \circ ” the Schur product. This function is defined in the time interval $t \in (t_i, t_f)$ where the target motion occurs, and t_δ is defined in (35). The value of $\bar{\theta}_{xi}$ and $\underline{\theta}_{xi}$ over time are

$$\begin{aligned} \underline{\theta}_{xi} &= (\underline{\theta}_i - \theta_{0i} + |\underline{\theta}_i - \theta_{0i}|) / 2, \\ \bar{\theta}_{xi} &= (\bar{\theta}_i - \theta_{0i} - |\bar{\theta}_i - \theta_{0i}|) / 2. \end{aligned} \quad (41)$$

These values represent the area between θ_i and the limits of the FOV constraints, $\bar{\theta}_i$ and $\underline{\theta}_i$, when θ_i is outside these limit constraints. Parameters a and c are real constants to be found with the following optimization

$$\arg \min_{a,c} \int_{t_i}^{t_f} |\theta_{0i} - \theta_{gi}| dt, \quad (42)$$

subject to: $a, c \in \mathcal{R}^+$, $|\beta_{ri}| \leq \beta$.

The goal of this optimization is to find the values of a and c that bring θ_{gi} as close as possible to the predefined value θ_{0i} within the limits of FOV constraints (25) and without violating formation and motion constraints.

This variable formation angles strategy is illustrated in Fig. 8 (top-right, and third row) following again the previous example in which the target follows an ellipsoidal motion and the robots form a regular pentagon with $\beta = 30 \text{ deg.}$ and $d_0 = 5 \text{ m}$. This strategy performs similar to the previous one (Section IV-C) and the main difference can be seen in the left plots in second and third row of Fig. 8, where the thin solid lines represent the proposed evolution of θ_{ci} and θ_{ri} , respectively. It can be seen that the FOV constraints are respected and, in the second strategy, some values of θ_{ri} are constant since their adaptation from their predefined values (θ_{0i}) is not required to satisfy the FOV constraints.

The previous strategies are based either on adaptive scale or on adaptive angles. Therefore, while we adapt the formation in order to fit the problem’s constraints, we still preserve either the size or shape of the formation. This fits the assumption that lies at the core of *formation control* problems, that the geometric parameters that define the prescribed formation provide key advantages. However, other alternatives can be devised, such as adapting scale and angles simultaneously to increase the flexibility of the method. For example, the optimization problem could be defined with a combination of the corresponding cost functions (36) and (42) as follows

$$\arg \max_{a,c} \int_{t_i}^{t_f} \alpha (\kappa_L - \kappa_r) + (1 - \alpha) |\theta_{0i} - \theta_{gi}| dt, \quad (43)$$

subject to: $a, c \in \mathcal{R}^+$, $|\beta_{ri}| \leq \beta$,

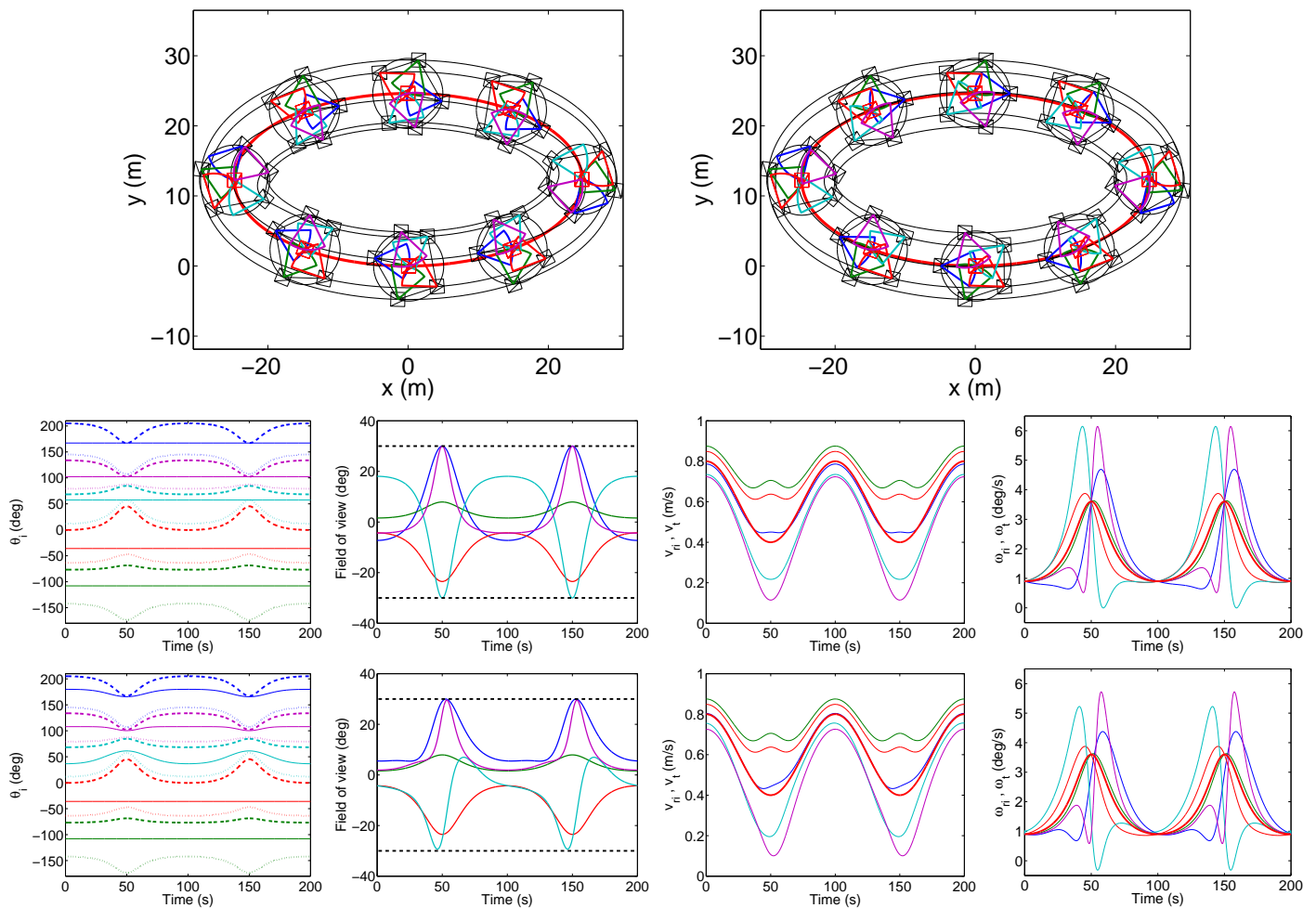


Fig. 8. Example of Fig. 3 using the strategy of constant formation angles presented in Section IV-C (top-left and second row) and the strategy of variable formation angles presented in Section IV-D (top-right and third row). Top: motion of the robots. Second and third row, from left to right: (first column) evolution of the FOV constraints defined for θ_i in *Case 4* and the proposed strategies: θ_{ci} (37) and θ_{ri} (39). For each i , the lower and upper limits are plotted in dotted and dashed lines, respectively. Thin lines are the proposed evolution of θ_i that must be within these limits; (second column) projection angle of the target in the FOV of each camera β_{ti} ; (third column) linear velocities v_{ri} of all the robots and the target v_t ; (fourth column) angular velocities ω_{ri} of all the robots and the target ω_t . Target velocities are in thicker line. It can be seen that both strategies, using respectively constraints (37) and (39), respect the FOV limits.

where $\alpha \in [0, 1]$ is a real number to weight the influence of each term. Note that the case of $\alpha = 0$ and $\alpha = 1$ corresponds to the strategies IV-B and IV-D, respectively.

E. Analysis of robustness

In this section, we study empirically the effect of noisy measurements and latency in the method performance. For simplicity, we consider the previous example in which the target follows an ellipsoidal motion and the robots form a regular pentagon with $\beta = 30 \text{ deg}$, but note that the results are consistent with different number of robots or target trajectories. The following tests are performed adding Gaussian random noise with mean 0 and standard deviation σ to the target evolution estimation used in the proposed strategies. In particular, we add noise to v_t with $\sigma_v = \sigma/10^3$ and to ω_t with $\sigma_\omega = \sigma/10^4$ for $\sigma = 0, 1, \dots, 10$. For example, $\sigma = 10$ produces a perturbation of 1 cm/s and approximately 0.06 deg/s (note that the maximum values of v_t and ω_t are respectively around 0.8m/s and 3.5deg/s as can be seen, for

example, in Fig. 3). For each value of σ , 100 repetitions are performed and the statistical results are represented with box-plots. Each box-plot shows the median of the data, the lower and upper quartiles, two *whiskers* representing the variability outside quartiles, and the outliers as individual crosses.

The results using the four different strategies proposed in Sections IV-A to IV-D are presented in Fig. 9. These strategies were designed to adjust exactly to the limits of the FOV constraints (see case of $\sigma = 0$ in Fig. 9(a)(c), where the minimum values of the difference between β and $|\beta_{ri}(\sigma)|$ are given). As the results show, due to the presence of noise, in practice the strategies need to be more conservative to fulfill the constraints. That is to say, the value of FOV limit used to compute the parameters (d_r or θ_{ri}) of the strategies has to be smaller than the nominal one (β). This smaller FOV provides a safety margin. In particular, the higher the noise the more the formation scale needs to be reduced by the strategy. This can be seen in Fig. 9(b), where for each repetition the maximum values of the difference between $d_c(\sigma = 0)$ and $d_c(\sigma)$ are

depicted (i.e., it represents the reduction of the formation scale that maintains FOV constraints). This reduction of the scale implies larger margins with respect to the FOV limits, whereas the strategy adjusts the FOV limits with $\sigma = 0$, see (a). Similar reasoning can be made in (c)-(d), where this time, the maximum values of the difference between $\theta_{ci}(\sigma = 0)$ and $\theta_{ci}(\sigma)$ are depicted in (d). In these previous tests, the strategies tackle the presence of noise by adapting the formation parameters to respect FOV limits. A different test is presented in the last row of Fig. 9. There, the strategies are calculated with ideal data with zero noise despite the actual noise of the target velocities. Then, since the effect of noise is not taken into account, performance deteriorates with respect to the previous tests. These last tests illustrate what happens if the strategy is computed with a priori information about the target motion without taking into account noise and without using safety margins in the FOV limits. The minimum values of β minus $|\beta_{ri}(\sigma)|$ are given in (e)-(f). Negative values mean that the target leaves the FOV. In summary, the tests show that more noise requires increasing the safety margin by reducing the nominal FOV and then, the flexibility of the strategy is reduced. The data in Fig. 9(a) and (c) also shows the reduction in degrees of the FOV that allows to deal with noise. In other words, it gives an idea of the safety margin in the FOV that should be used in the presence of noise.

Another perturbation that may affect the performance of the system is the latency of the estimations. Time delays arising in practice include those associated with the acquisition of information through the camera and its processing. The results of the proposed strategies in the presence of time delays ($\tau = 0, 1, \dots, 10$ s) are given in Fig. 10. For each value of time delay τ , the box-plots show the angular position of the target in the cameras' FOV along the simulation without delays, $\beta_{ri}(\tau = 0)$, minus the case with delays $\beta_{ri}(\tau)$. The simulation time was 200s with time step of 0.1s. When time delay increases, it can be seen that the values of $\beta_{ri}(\tau)$ grow with respect to $\beta_{ri}(\tau = 0)$, i.e. the image projection of the target approaches to the FOV limits. Eventually, the target may leave the FOV for some time as shown in the plotted lines with dots, which show for each τ the maximum value of $|\beta_{ri}|$. For $\tau = 0$, the target projection does not exceed the FOV limits ($\beta = 30deg$), whereas for increasing τ the target will leave the FOV at some instants. Therefore, due to the presence of time delays, the strategies also need to be more conservative to fulfill the constraints by reducing the effective FOV to provide a safety margin. Note that the effect of time delays is directly related with the target trajectory. If the target motion is smooth the perturbation effect is reduced whereas aggressive manoeuvres of the target produce greater changes in v_t and ω_t and a higher deterioration of the system performance due to time delays.

F. Constraints with target size and collision avoidance

In practical applications, the size of the target may require to be considered. Next, we extend the proposed strategies taking into account the size of the target. Let us consider the target size is defined with a circle of radius R . This magnitude is projected in the robot's camera as β_R . Considering the

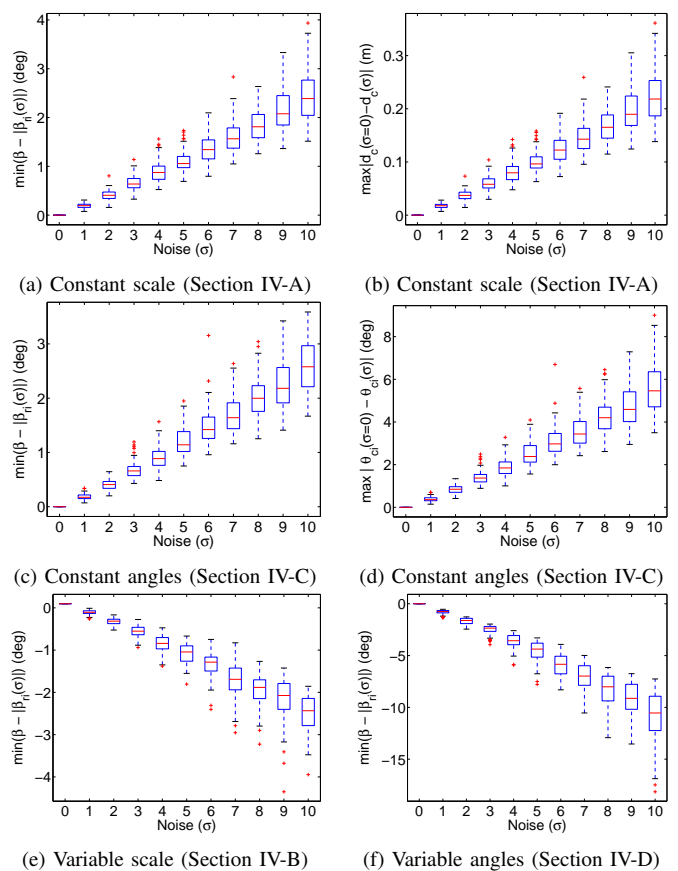


Fig. 9. System performance in the presence of noise for each strategy. Box-plots in (a), (c), (e) and (f) show the minimum values of the difference between β and $|\beta_{ri}(\sigma)|$. Box-plots in (b), and (d) respectively, represent the maximum differences between $d_c(\sigma)$ ($\theta_{ci}(\sigma)$) with respect to the case without noise $d_c(\sigma = 0)$ ($\theta_{ci}(\sigma = 0)$). Positive values in (a) and (c) mean the FOV constraint is respected, whereas negative values in (e) and (f) mean that FOV constraint is violated. See the text for detailed interpretation.

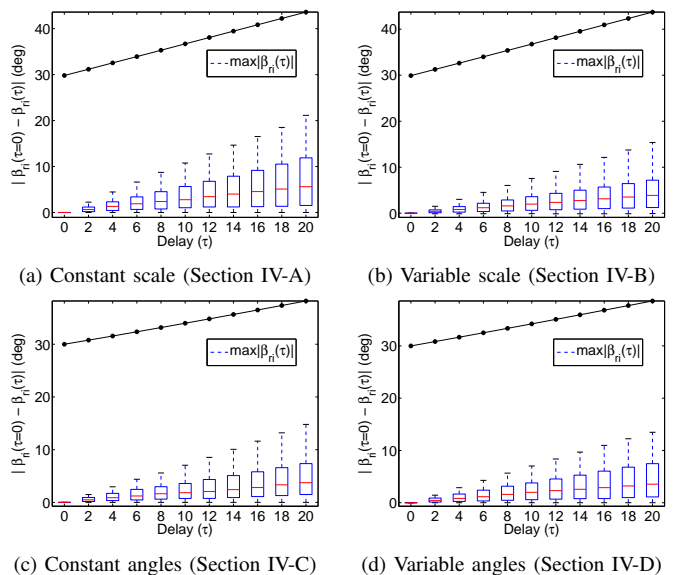


Fig. 10. Performance in the presence of time delays. Each figure (a)-(d) corresponds to a different strategy. For each value of time delay τ , the box-plot shows the difference between the angular position of the target in the cameras' FOV along the simulation without delays, $\beta_{ri}(\tau = 0)$, with respect to the case with delays $\beta_{ri}(\tau)$. Additionally, the line with dots shows the maximum value of $|\beta_{ri}|$ for each τ .

triangle defined by the camera and target with opposite side R and hypotenuse d_i , the value of β_R can be computed as $\tan(\beta_R) = R/\sqrt{d_i^2 - R^2}$ with d_i the distance to the target. Then, to ensure the target will remain within view, we reduce the limit angle β of the FOV as $(\beta - \beta_R)$.

On the one hand, this constraint limits the minimum distance of the robot to the target since with small distances the target may fill the full FOV of the camera. In particular, this imposes an upper limit κ_U , given by $\kappa_U = \sin(\beta)/R$. On the other hand, taking into account this additional constraint in (20) yields

$$d_c = \frac{1}{\kappa_c} \leq d_i = \frac{1}{\kappa_i} = \left| \frac{v_t \sin(\pm(\beta - \beta_R))}{\omega_t \cos(\pm(\beta - \beta_R) - \theta_{0i})} \right|. \quad (44)$$

The worst case of κ_i is $\kappa_{wc}(t) = \max_i(\kappa_i)$ and its maximum value is $\kappa_L = \max_t(\kappa_{wc})$. Then, extension of strategy in Section IV-A yields that any constant value κ_c such that $\kappa_L \leq \kappa_c \leq \kappa_U$ will obey FOV constraints. Implementation of strategy in Section IV-B also requires to modify constraint (18) as $|\tan \beta_{ri}| \leq |\tan(\pm(\beta - \beta_R))|$ with $i = 1, \dots, N$. Regarding strategies in Section IV-C and IV-D they can be directly applied by considering the new FOV limits $\pm(\beta - \beta_R)$.

Since, in reality, robots and target will have a certain physical size, collisions between them must be prevented. We define the additional constraints to guarantee collision avoidance with the target and between the robots. Collision of the robots with the target is avoided if $d_i \geq d_{min}$ where $d_{min} = R_t + R_r$ is the required minimum distance for safety between the centers of the agents, where R_t and R_r are the safety radii around the target and robot, respectively. Inter-robot collisions need to be considered only between robots that are physical neighbors in the formation, with $d_{min} = 2R_r$, and there are two different cases. The first is the case in which the formation scale is allowed to change (strategies in Sections IV-A and IV-B). In this case, the smaller the scale of the formation, the closer the robots are between them. From geometry, we have the following constraint to avoid inter-robot collisions:

$$d = d_i \geq \frac{d_{min}}{2 \sin(|\theta_{0i} - \theta_{0j}|/2)}, \quad (45)$$

with $j = i + 1$ for $i = 1, \dots, N - 1$ and $j = 1$ for $i = N$. The second case refers to the strategy in which the scale of the formation is fixed and the robots can change their angular pose in the formation (strategies in Sections IV-C and IV-D). In this case, collisions are avoided with the following constraint:

$$|\theta_i - \theta_j| \geq 2 \arcsin \frac{d_{min}}{2d_0}, \quad (46)$$

with $j = i + 1$ for $i = 1, \dots, N - 1$ and $j = 1$ for $i = N$. By checking these additional conditions in the strategies proposed earlier in Section IV we can guarantee that there will be no collisions between the robots or with the target. Notice that including these conditions of collision avoidance reduces the solution space. In that case, the existence of solution depends on the size of the agents and is not guaranteed.

G. Required information for strategy implementation

Strategies presented in Sections IV-A and IV-C only require to know in advance the value of $\kappa_{t_{max}}$ (i.e. the maximum allowed curvature of the target's trajectory), whereas strategies presented in Sections IV-B and IV-D also require to know in advance the full evolution of the target's velocities (v_t and ω_t). Additionally, all the presented strategies need the estimation of the current velocities of the target (e.g. by means of a state observer implemented in each robot) to perform a tracking control able to follow the proposed reference trajectories in real time while overcoming possible perturbations such as noise in the measurements.

The proposed formulation is based on relative position measurements to compute the robots' velocities. Examples of methods that estimate the position of a target using visual relative measurements can be found in [13] or [34]. A different approach is to use artificial markers, providing that adding markers on the target is allowed, in a similar way to [35]. It is clear from (12)-(13) that the robots can implement the strategy we propose using the measurements expressed in their own independent local coordinate frames, without requiring any common reference. Therefore, there is no need of communications between the robots.

V. CONCLUSION

In this paper, we have addressed the task of enclosing and tracking a dynamic target with the goal of keeping a prescribed formation pattern around this target. In particular, we have considered the problem of planning feasible paths for a set of unicycle robots mounting vision sensors with limited FOV. Therefore, the robots must follow appropriate trajectories to maintain visibility of the target throughout their motion. A video attachment presents several simulations to facilitate the understanding of how the system evolves with the different proposed strategies. The different strategies are implemented in *Matlab*® and the code is also provided as attached material to facilitate evaluation and reproducibility of the proposal.

In this approach, we use circular formations for enclosing the target. Simplicity and lack of occlusions are two of the advantages of this choice. Notice however that the target is not restricted to be in the centroid of the formation and our approach can be applied to any formation. In particular, any formation shape can be defined in polar coordinates with the location of each robot with respect to the target (distance d_i and angle θ_i). Then, we can use for instance the proposed strategies to compute the scale factor d_i for each robot, and then impose the worst-case value to all the robots or, alternatively, we can modify the angles θ_i in the formation while keeping the different prescribed constant distances of each robot with the target.

We have proposed different strategies for the definition of the adaptive formation. On the one hand, the scale of the formation is adapted so the problem constraints are fulfilled by defining appropriate robot trajectories. Existence of solution is guaranteed with this strategy. On the other hand, some applications may require to maintain a fixed scale. For example, for safety or accuracy issues the distance between the robots

and the target must be certain constant value. In that case, we propose another strategy in which the robots are allowed to modify their relative position in the formation but keeping a constant distance with the target. In order to design the strategies of variable scale or angles of the formation, we defined Gaussian-based functions. If there exist solutions to the problem, our strategy using Gaussian-based functions is guaranteed to provide a solution.

The presented simulations illustrate the correct performance of the approach as well as its versatility, which could be used to define additional strategies for solving new tasks. For example, the task of obstacle avoidance could be implemented if obstacle perception capabilities are available. The video attachment shows an illustrative example in which the robot formation tracks the target through a narrow corridor.

In the framework considered here, a fixed camera with limited FOV is set on each robot. This configuration is easy and robust to implement, and the FOV limitation is overcome with the proposed strategies. Some alternatives to avoid FOV constraints could be the use of a rotating camera on each robot, or omnidirectional vision. However, these options add hardware complexity, weight, or cost to the system, apart from the additional complexity of processing image information of non-standard camera systems.

REFERENCES

- [1] C. Robin and S. Lacroix, "Multi-robot target detection and tracking: taxonomy and survey," *Autonomous Robots*, vol. 40, no. 4, pp. 729–760, 2016.
- [2] G. Guerra-Filho, "Optical motion capture: Theory and implementation," *Journal of Theoretical and Applied Informatics*, vol. 12, no. 2, pp. 61–89, 2005.
- [3] G. Arechavaleta, J.-P. Laumond, H. Hicheur, and A. Berthoz, "On the nonholonomic nature of human locomotion," *Autonomous Robots*, vol. 25, pp. 25–35, 2008.
- [4] K. Zhou and S. I. Roumeliotis, "Multirobot active target tracking with combinations of relative observations," *IEEE Transactions on Robotics*, vol. 27, no. 4, pp. 678–695, August 2011.
- [5] P. Tokekar, V. Isler, and A. Franchi, "Multi-target visual tracking with aerial robots," in *IEEE/RSJ International Conference on Intelligent Robots and Systems*, September 2014, pp. 3067–3072.
- [6] Z. Wang and D. Gu, "Cooperative target tracking control of multiple robots," *IEEE Transactions on Industrial Electronics*, vol. 59, no. 8, pp. 3232–3240, August 2012.
- [7] F. Poiesi and A. Cavallaro, "Distributed vision-based flying cameras to film a moving target," in *IEEE/RSJ International Conference on Intelligent Robots and Systems*, September 2015, pp. 2453–2459.
- [8] G. Antonelli, F. Arrichiello, and S. Chiaverini, "The entrapment/escorting mission," *IEEE Robotics & Automation Magazine*, vol. 15, no. 1, pp. 22–29, 2008.
- [9] R. Sepulchre, D. Paley, and N. Leonard, "Stabilization of planar collective motion: All-to-all communication," *IEEE Transactions on Automatic Control*, vol. 52, no. 5, pp. 811–824, May 2007.
- [10] N. Moshtagh, N. Michael, A. Jadbabaie, and K. Daniilidis, "Vision-based, distributed control laws for motion coordination of nonholonomic robots," *IEEE Transactions on Robotics*, vol. 25, no. 4, pp. 851–860, 2009.
- [11] A. Marasco, S. Givigi, and C.-A. Rabbath, "Model predictive control for the dynamic encirclement of a target," in *American Control Conference*, 2012, pp. 2004–2009.
- [12] M. Aranda, G. López-Nicolás, C. Sagüés, and M. M. Zavlanos, "Three-dimensional multirobot formation control for target enclosing," in *IEEE/RSJ International Conference on Intelligent Robots and Systems*, September 2014, pp. 357–362.
- [13] M. Deghat, I. Shames, B. D. O. Anderson, and C. Yu, "Localization and circumnavigation of a slowly moving target using bearing measurements," *IEEE Transactions on Automatic Control*, vol. 59, no. 8, pp. 2182–2188, August 2014.
- [14] A. Franchi, P. Stegagno, and G. Oriolo, "Decentralized multi-robot encirclement of a 3D target with guaranteed collision avoidance," *Autonomous Robots*, vol. 40, no. 2, pp. 245–265, 2016.
- [15] A. Franchi, P. Stegagno, M. D. Rocco, and G. Oriolo, "Distributed target localization and encirclement with a multi-robot system," in *7th IFAC Symposium on Intelligent Autonomous Vehicles*, 2010.
- [16] Y. Lan, Z. Lin, M. Cao, and G. Yan, "A distributed reconfigurable control law for escorting and patrolling missions using teams of unicycles," in *IEEE Conference on Decision and Control*, 2010, pp. 5456–5461.
- [17] Z. Sun, M.-C. Park, B. D. Anderson, and H.-S. Ahn, "Distributed stabilization control of rigid formations with prescribed orientation," *Automatica*, vol. 78, pp. 250–257, 2017.
- [18] L. Krick, M. Broucke, and B. Francis, "Stabilisation of infinitesimally rigid formations of multi-robot networks," *International Journal of Control*, vol. 82, no. 3, pp. 423–439, 2009.
- [19] H. G. de Marina, M. Cao, and B. Jayawardhana, "Controlling rigid formations of mobile agents under inconsistent measurements," *IEEE Transactions on Robotics*, vol. 31, no. 1, pp. 31–39, 2015.
- [20] S. Ramazani, R. Selmic, and M. de Queiroz, "Rigidity-based multiagent layered formation control," *IEEE Transactions on Cybernetics*, vol. 47, no. 8, pp. 1902–1913, August 2017.
- [21] K.-K. Oh, M.-C. Park, and H.-S. Ahn, "A survey of multi-agent formation control," *Automatica*, vol. 53, pp. 424–440, March 2015.
- [22] G. Kantor and A. Rizzi, "Feedback control of underactuated systems via sequential composition: Visually guided control of a unicycle," in *Proc. of 11th Int. Symposium of Robotics Research*, 2003.
- [23] P. Murrieri, D. Fontanelli, and A. Bicchi, "A hybrid-control approach to the parking problem of a wheeled vehicle using limited view-angle visual feedback," *International Journal of Robotics Research*, vol. 23, no. 4-5, pp. 437–448, April-May 2004.
- [24] S. Bhattacharya, R. Murrieta-Cid, and S. Hutchinson, "Optimal paths for landmark-based navigation by differential-drive vehicles with field-of-view constraints," *IEEE Transactions on Robotics*, vol. 23, no. 1, pp. 47–59, 2007.
- [25] P. Salaris, D. Fontanelli, L. Pallottino, and A. Bicchi, "Shortest paths for a robot with nonholonomic and field-of-view constraints," *IEEE Transactions on Robotics*, vol. 26, no. 2, pp. 269–281, April 2010.
- [26] G. López-Nicolás, N. R. Gans, S. Bhattacharya, C. Sagüés, J. J. Guerrero, and S. Hutchinson, "Homography-based control scheme for mobile robots with nonholonomic and field-of-view constraints," *IEEE Transactions on Systems, Man, and Cybernetics, Part B (Cybernetics)*, vol. 40, no. 4, pp. 1115–1127, August 2010.
- [27] P. Salaris, L. Pallottino, and A. Bicchi, "Shortest paths for finned, winged, legged, and wheeled vehicles with side-looking sensors," *International Journal of Robotics Research*, vol. 31, no. 8, pp. 997–1017, 2012.
- [28] A. Cristofaro, P. Salaris, L. Pallottino, F. Giannoni, and A. Bicchi, "On time-optimal trajectories for differential drive vehicles with field-of-view constraints," in *53rd IEEE Conference on Decision and Control*, Dec 2014, pp. 2191–2197.
- [29] J.-B. Hayet, H. Carlos, C. Esteves, and R. Murrieta-Cid, "Motion planning for maintaining landmarks visibility with a differential drive robot," *Robotics and Autonomous Systems*, vol. 62, no. 4, pp. 456–473, 2014.
- [30] T. Nageli, J. Alonso-Mora, A. Domahidi, D. Rus, and O. Hilliges, "Real-time motion planning for aerial videography with dynamic obstacle avoidance and viewpoint optimization," *IEEE Robotics and Automation Letters*, vol. 2, no. 3, pp. 1696–1703, July 2017.
- [31] M. M. Asadi, A. Ajorlou, and A. G. Aghdam, "Cooperative control of multi-agent systems with limited angular field of view," in *American Control Conference*, June 2012, pp. 2388–2393.
- [32] D. Panagou and V. Kumar, "Cooperative visibility maintenance for leader-follower formations in obstacle environments," *IEEE Transactions on Robotics*, vol. 30, no. 4, pp. 831–844, August 2014.
- [33] G. López-Nicolás, M. Aranda, and Y. Mezouar, "Formation of differential-drive vehicles with field-of-view constraints for enclosing a moving target," in *IEEE International Conference on Robotics and Automation*, 2017, pp. 261–266.
- [34] A. K. Das, R. Fierro, V. Kumar, J. P. Ostrowski, J. Spletzer, and C. J. Taylor, "A vision-based formation control framework," *IEEE Trans. on Robotics and Automation*, vol. 18, no. 5, pp. 813–825, 2002.
- [35] G. López-Nicolás, N. R. Gans, S. Bhattacharya, J. J. Guerrero, C. Sagüés, and S. Hutchinson, "Homography-based control scheme for mobile robots with nonholonomic and field-of-view constraints," *IEEE Trans. on Sys., Man, and Cybern., Part B: Cybern.*, vol. 40, no. 4, pp. 1115–1127, 2010.